

---

# MISSINGNESS BIAS CALIBRATION IN FEATURE ATTRIBUTION EXPLANATIONS

000  
001  
002  
003  
004  
005 **Anonymous authors**  
006 Paper under double-blind review  
007  
008  
009  
010

## ABSTRACT

011 Popular explanation methods often produce unreliable feature importance scores  
012 due to “missingness bias,” a systematic distortion that arises when models are  
013 probed with ablated, out-of-distribution inputs. Existing solutions treat this as a  
014 deep representational flaw that requires expensive retraining or architectural mod-  
015ifications. In this work, we challenge this assumption and show that missingness  
016 bias can be effectively treated as a superficial artifact of the model’s output space.  
017 We introduce MCAL, a lightweight post-hoc method that corrects this bias by fine-  
018 tuning a simple linear head on the outputs of a frozen base model. Surprisingly,  
019 we find this simple correction consistently reduces missingness bias and is com-  
020 petitive with, or even outperforms, prior heavyweight approaches across diverse  
021 medical benchmarks spanning vision, language, and tabular domains.  
022  
023

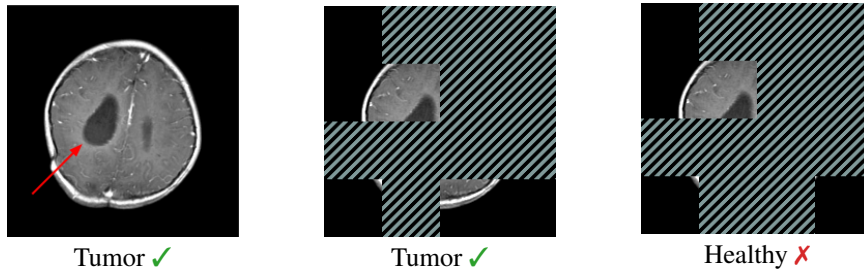
## 1 INTRODUCTION

024 As black-box deep learning systems are increasingly deployed in high-stakes settings such as  
025 medicine, finance, and law, there is increasing demand for reliable and trustworthy model expla-  
026 nations. A common approach for explaining model predictions is to use feature attribution methods,  
027 which assign importance scores to input features based on their influence on the output. Popular  
028 methods, such as LIME (Ribeiro et al., 2016) and SHAP (Lundberg & Lee, 2017), estimate these  
029 scores by perturbing the input, typically by ablating selected features and measuring the change in  
030 prediction. Because true feature removal is often infeasible (e.g., one cannot physically delete im-  
031 age pixels or omit words from tokenized sequences), attribution methods approximate removal by  
032 substituting the selected features with default or placeholder values, such as black pixels or special  
033 tokens (Ancona et al., 2017; Sundararajan et al., 2017).

034 These substitutions often result in out-of-distribution inputs that deviate significantly from the  
035 model’s training data, inducing a systematic distortion in predictions known as *missingness*  
036 *bias* (Hase et al., 2021; Hooker et al., 2019; Jain et al., 2022). Such bias can severely undermine the  
037 reliability of explanations. As illustrated in Figure 1, a classifier that accurately detects a brain tumor  
038 from clean inputs fails to do so when irrelevant features are masked, demonstrating how seemingly  
039 innocuous ablations can corrupt model behavior. Since perturbation-based attributions are derived  
040 directly from these corrupted predictions, their reliability is fundamentally compromised, leading  
041 to inconsistent feature importance scores (Duan et al., 2024; Goldwasser & Hooker, 2024; Hooker  
042 et al., 2019). This also opens the door to adversarial manipulation: malicious actors can exploit this  
043 vulnerability to design deceptive models that obscure their use of sensitive attributes such as race or  
044 gender (Joe et al., 2022; Koyuncu et al., 2024; Slack et al., 2020).

045 A variety of mitigation strategies have been proposed to address missingness bias. *Replacement-*  
046 *based* methods aim to reduce distributional shift by imputing masked features with more realistic  
047 content (Agarwal & Nguyen, 2020; Chang et al., 2018; Kim et al., 2020; Sturmels et al., 2020).  
048 *Training-based* methods fine-tune or retrain the model to better handle ablations (Hase et al., 2021;  
049 Hooker et al., 2019; Park et al., 2024; Rong et al., 2022), while *architecture-based* approaches embed  
050 robustness directly into the model via structural design changes (Balasubramanian & Feizi, 2023;  
051 Jain et al., 2022).

052 However, these strategies are often impractical. Replacement-based methods are usually specialized  
053 to specific domains (e.g., text (Kim et al., 2020)) or might require training model-specific imputa-  
054 tions (Chang et al., 2018). On the other hand, training-based solutions require intensive engineering



054  
055  
056  
057  
058  
059  
060  
061  
062  
063  
064  
065  
066  
067  
068  
069  
070  
071  
072  
073  
074  
075  
076  
077  
078  
079  
080  
081  
082  
083  
084  
085  
086  
087  
088  
089  
090  
091  
092  
093  
094  
095  
096  
097  
098  
099  
100  
101  
102  
103  
104  
105  
106  
107  
Figure 1: **Removing irrelevant features can cause a misdiagnosis.** A fine-tuned ViT (Dosovitskiy et al., 2020) correctly predicts “tumor” on the clean image (left) and a subset of the relevant features (middle). However, masking irrelevant features flips the prediction to “healthy”, despite the tumor remaining visible (right). For visualization, gray stripes denote zero-valued pixels, and images are contrast-boosted.

and computing resources, while architecture-based modifications require a deep understanding of model internals. Moreover, it is also increasingly common that the model itself is a black-box, such as when interacting with API-based LLM providers.

In this work, we question whether such complex interventions are necessary. We investigate a simple yet surprisingly powerful strategy for mitigating missingness bias: finetuning a linear head on the outputs of a frozen base model. This approach, which we call **MCal**, is *lightweight, model-agnostic*, and *post-hoc*: it is significantly cheaper in implementation effort than training-based methods, does not require model-specific adaptations like architecture-based and replacement-based methods, and needs only access to the model’s output logits. In the following, we summarize the development of MCal and our contributions.

**A New Perspective on Missingness Bias.** We find that missingness bias, a problem often treated as a deep representational flaw, can be effectively mitigated with a simple post-hoc correction in the model’s output space. This finding suggests the bias is often a superficial artifact, challenging the prevailing assumption that expensive retraining or architectural modifications are necessary.

**A Lightweight Method with Theoretical Guarantees.** We formalize this approach as MCal, a lightweight calibrator that is highly efficient to optimize (Section 3). Furthermore, our simple formulation provides theoretical guarantees of convergence to a globally optimal solution, ensuring a level of stability and reproducibility rare for deep learning interventions.

**A Strong and Practical Baseline.** We demonstrate MCal’s effectiveness across diverse models and data modalities, where it is often competitive with heavyweight approaches (Section 4). This establishes a strong and practical baseline that can be immediately adopted by researchers and practitioners to improve the reliability of their explanations.

## 2 UNDERSTANDING MISSINGNESS BIAS

Perturbation-based feature attribution methods like LIME (Ribeiro et al., 2016) and SHAP (Lundberg & Lee, 2017) evaluate models on inputs with ablated features, typically replaced by fixed baseline values (e.g., zero-vectors or mean-pixel values). However, because these synthetic inputs often fall outside the model’s training distribution, they can induce systematic prediction distortions, a phenomenon known as *missingness bias*. This section provides a background on this bias and its consequences for explanation reliability.

### 2.1 PATHOLOGY: SYMPTOMS AND MEASUREMENTS

The effects of missingness bias are not merely statistical curiosities; they manifest as tangible failures that undermine the reliability of explanation methods.

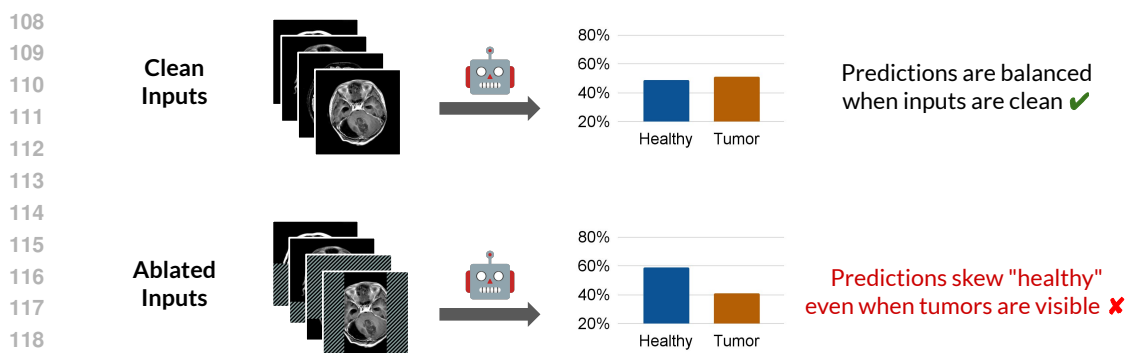


Figure 2: **Feature ablations induce class distribution shifts.** Masking non-critical regions skews predictions towards the “healthy” class, even when tumors remain visible. This effect, known as *missingness bias*, causes the model to misclassify inputs that retain relevant features, and undermines the reliability of feature attribution explanations.

**Systematic Skew in Predictions.** The most direct failure mode of missingness bias is a systematic skew in model predictions (Jain et al., 2022). As illustrated in Figure 2, the model’s accuracy degradation is not random but systematic: it develops a consistent bias towards one class (in this case, “healthy”) even when the core evidence for the correct class remains visible. This failure mode is particularly pernicious, persisting even when we selectively avoid masking the central image patches most likely to contain the tumor.

**Unreliable Feature Attributions.** Another consequence of this degraded accuracy is that any feature attributions derived from the model are fundamentally unreliable. If a model’s predictions are incorrect on ablated inputs, the importance scores computed from these predictions cannot be trusted to reflect the model’s true reasoning. Empirical findings support this; for instance, Jain et al. (2022) show that feature importance scores from models with high missingness bias fail standard robustness tests such as top- $k$  removal. Prior work has also shown that minor changes to the ablation process can yield vastly different explanations, suggesting they reflect perturbation artifacts rather than genuine model logic (Hooker et al., 2019).

**Quantifying Missingness Bias.** Many feature attribution methods operate under the assumption that feature ablation is a neutral act of intervention intended to simulate the removal of information (Sturmels et al., 2020; Sundararajan et al., 2017). When a model’s behavior deviates from this expected neutrality, the resulting shift in its aggregate predictive distribution serves as a direct measure of missingness bias. This shift is typically quantified as the distribution shift between the class frequencies on the clean data distribution  $\mathcal{D}$  versus the ablated data distribution  $\mathcal{D}'$  (Balasubramanian & Feizi, 2023; Jain et al., 2022):

$$\text{MissingnessBias}(f) = D_{\text{KL}} \left( \mathbb{E}_{x' \sim \mathcal{D}'} \text{Class}(f(x')) \parallel \mathbb{E}_{x \sim \mathcal{D}} \text{Class}(f(x)) \right), \quad (1)$$

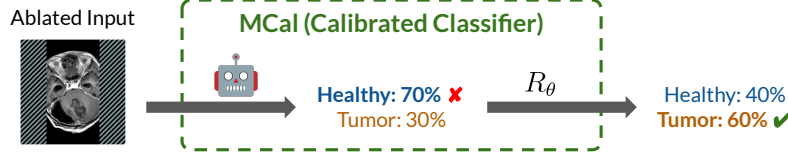
where  $\mathcal{D}'$  is the distribution of inputs where each feature is i.i.d. ablated with some given probability, and let  $\text{Class}(f(x))$  be the one-hot vector representation of the class predicted by  $f$  on  $x$ . The above can then be understood as a measure of information-theoretic “surprise” when  $f$  is evaluated on *unbiased* ablations, supposing only knowledge of its behavior on clean inputs. In particular, Jain et al. (2022) specifically introduces this to measure missingness bias, rather than of adjacent phenomena, such as prediction sensitivity with respect to top- $k$  feature selections (Hase et al., 2021).

## 2.2 THE CHALLENGE OF MITIGATION

A variety of strategies have been proposed to address missingness bias, which can be broadly categorized as follows:

- *Replacement-based.* These methods aim to make ablated inputs appear more in-distribution. Beyond simple values (e.g., zero and mean-valued (Hase et al., 2021)), more complex variants include marginalization, which averages outputs over plausible replacement values (Chirkova

162  
163  
164  
165  
166  
167



168 Figure 3: **MCAL corrects class distribution shifts induced by input ablations.** The ablated input  
169 initially predicts “healthy”. MCAL applies a learned transformation  $R_\theta$  to adjust the output proba-  
170 bilities, thereby restoring alignment with expected class distributions. This calibration method is  
171 model-agnostic, requiring only the classifier’s output probabilities of each class.  
172  
173

174 et al., 2023; Frye et al., 2020; Haug et al., 2021; Kim et al., 2020; Vo et al., 2024), random  
175 noising (Rong et al., 2022), and generative modeling, which uses a secondary model to in-paint  
176 realistic content (Agarwal & Nguyen, 2020; Chang et al., 2018). However, these approaches are  
177 often computationally expensive and can introduce their own artifacts.  
178

- *Training-based.* This approach treats feature ablations as a form of data augmentation. Methods like ROAR (Hooker et al., 2019) and GOAR (Park et al., 2024) retrain or fine-tune the model on masked inputs to align its train and test distributions. Although effective at building robust representations, this strategy is computationally expensive and only possible when the model can be modified.
- *Architecture-based.* These methods embed robustness directly into the model’s design. For example, modified vision transformers (Dosovitskiy et al., 2020; Jain et al., 2022) and CNNs (Balasubramanian & Feizi, 2023) can be altered to use dedicated mask tokens or explicitly suppress the influence of ablated regions. However, these changes are often non-trivial, architecture-specific, and not generalizable.

187 While often effective, the high cost and complexity of these methods make them impractical for  
188 many modern use cases, especially those involving large-scale, pre-trained foundation models. Fur-  
189 thermore, such approaches are entirely infeasible when working with API-based models that do not  
190 permit retraining or architectural changes. This gap highlights the need for a practical, lightweight,  
191 and model-agnostic approach to mitigating missingness bias that we introduce next.  
192

### 193 3 MCAL: A LIGHTWEIGHT CALIBRATOR FOR MISSINGNESS BIAS

195 Having established the pathology of missingness bias and the practical limitations of existing heavy-  
196 weight solutions, we now introduce our method. We propose **MCAL**, a lightweight, post-hoc correc-  
197 tion that is surprisingly effective at mitigating missingness bias.  
198

#### 200 3.1 ARCHITECTURE AND OPTIMIZATION

201 The calibration process is illustrated in Figure 3. A base classifier  $f : \mathbb{R}^n \rightarrow \mathbb{R}^m$  first processes an  
202 input  $x$  to output the *raw logits*  $z = f(x)$ . A calibrator  $R_\theta : \mathbb{R}^m \rightarrow \mathbb{R}^m$  then transforms the raw  
203 logits into the *calibrated logits*  $R_\theta(z)$ . Specifically, we implement this as an affine transform:  
204

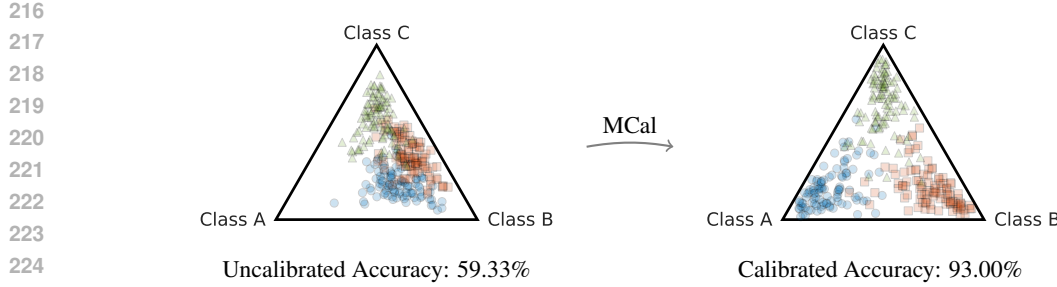
$$R_\theta(z) = Wz + b, \quad (2)$$

205 where the calibrator is parametrized by  $\theta = (W, b)$ , with  $W \in \mathbb{R}^{m \times m}$  and  $b \in \mathbb{R}^m$ . To fit the cali-  
206 brator, we use a standard cross-entropy objective that aligns the calibrated prediction on an ablated  
207 input with the base model’s prediction on the clean input:  
208

$$\mathcal{L}(\theta) = \mathbb{E}_{(x, x') \sim \mathcal{D}} \text{CrossEntropy}[R_\theta(f(x')), \text{Class}(f(x))], \quad (3)$$

209 where  $(x, x') \sim \mathcal{D}$  are samples of a clean input  $x$  and its ablated version  $x'$ , and  $\text{Class}(f(x))$  denotes  
210 the one-hot prediction on the clean input.  
211

212 Our approach is deliberately minimalist, prioritizing efficiency without compromising performance.  
213 We apply a standard cross-entropy objective, identical to that used in heavyweight retraining meth-  
214 ods (Hooker et al., 2019), but only to a lightweight matrix-scaling calibrator (Guo et al., 2017). This  
215



227 **Figure 4: Geometric intuition of MCal on a synthetic dataset.** Missingness bias causes the uncalibrated outputs to shift. For instance, the Class A cluster (blue circles) is pulled towards the Class 228 B vertex, leading to systematic misclassification and low accuracy. MCal applies an optimal affine 229 transformation to the uncalibrated outputs, correcting the shift and improving accuracy. 230

231  
232 design is highly efficient, with orders of magnitude fewer parameters ( $m^2 + m$ ) than fine-tuning or 233 even parameter-efficient methods like LoRA (Hu et al., 2022). Our experiments in Section 4 confirm 234 that this minimalist approach is, in fact, sufficient to yield competitive performance with more 235 engineering-intensive approaches like retraining the model or architecture modifications. Furthermore, 236 this simple design also comes with strong theoretical guarantees on its optimization process, 237 which we detail next.  
238

### 239 3.2 THEORETICAL GUARANTEES AND GEOMETRIC INTERPRETATION 240

241 Our affine parametrization of  $R_\theta$  means that standard gradient-based optimization will provably 242 converge to an optimal solution, which we formalize as follows.

243 **Theorem 3.1** (Guaranteed Optimal Convergence). *The MCal objective  $\mathcal{L}(\theta)$  is convex in  $\theta$ .*

244  
245 *Proof.* The function  $\mathcal{L}(\theta)$  is convex in  $\theta$ , as it is a composition of the convex cross-entropy loss and 246 an affine transformation. Because local minimums are also global minimums for convex functions, 247 standard gradient-based optimization (e.g., SGD, Adam) will converge to an optimal solution.  $\square$   
248

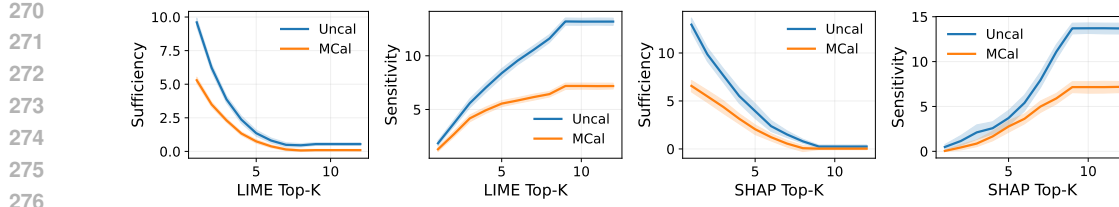
249 The importance of this guarantee is twofold. First, it ensures reproducibility and stability: the 250 optimization process is guaranteed to converge to the same optimal solution, reducing the need for 251 extensive hyperparameter sweeps or random seed searches. Second, it provides a strong assurance 252 of quality, guaranteeing that the resulting calibrator is a globally optimal affine correction for the 253 given data.  
254

**Geometric Interpretation.** MCal also has a clear geometric interpretation, visualized in Figure 4. 255 The uncalibrated outputs form biased point clouds on the probability simplex, with the Class A 256 cluster pulled towards the Class B vertex, leading to systematic misclassification. MCal learns an 257 optimal affine transformation in the logit space that rotates, scales, and shifts these distributions. 258 This untangles the clouds and pushes them towards their correct vertices. Theorem 3.1 guarantees 259 that this correction is globally optimal for our parametrization.  
260

### 261 3.3 IMPLEMENTATION CONSIDERATIONS 262

263 **Conditioning on Ablation Rates.** Our experience shows that the severity of missingness bias is 264 strongly correlated with the fraction of features that are ablated. To account for this, we recommend 265 using an “ensemble” of specialized calibrators, each one fit for a specific ablation rate (e.g., 10%, 266 20%, etc.). At inference time, we apply the calibrator that was trained for the ablation rate closest to 267 that of the input. We study the advantage of this ensemble in Section 4.  
268

**Integration with Explainers.** As a post-hoc wrapper, MCal is compatible with any perturbation-based explanation method. The calibrated model,  $f$ , can be used as a drop-in replacement for the  
269



270  
271  
272  
273  
274  
275  
276  
277 **Figure 5: Calibrated models have better explanations.** Compared to an uncalibrated baseline  
278 model (Uncal), LIME and SHAP explanations on MCal-calibrated models have more accurate fea-  
279 ture importance scores (sufficiency  $\downarrow$ ). In addition, calibrated models are also more robust to feature  
280 ablations (sensitivity  $\downarrow$ ). Results are shown for the MRI dataset using an unconditioned calibrator.  
281  
282

283 original model,  $f$ , in any existing explainability pipeline. The resulting feature attributions are then  
284 generated from a model that has been explicitly corrected for the missingness bias induced by the  
285 explanation method’s own perturbation strategy.

286  
287 **Training Set Size and Overfitting.** Dense parametrizations of  $W$  risk overfitting when the num-  
288 ber of parameters exceeds the number of training samples (Guo et al., 2017), which can occur when  
289 there are many classes. In such cases, the training loss may go to zero while test performance does  
290 not improve. We recommend two strategies to mitigate overfitting. First, one may consider adding  
291 a regularization term to the objective. Second, one may also consider sparse parametrizations, such  
292 as taking  $W$  to be a diagonal matrix (also known as “vector-scaling”), which would reduce the total  
293 parameter count to  $O(m)$ .  
294

## 295 4 EXPERIMENTS

296  
297 We now present experiments to validate the impact of missingness bias in explainability, as well  
298 as the ability of MCal to mitigate it. Moreover, we demonstrate that MCal repeatedly outperforms  
299 more expensive baselines, such as full retraining and architecture modifications. Additional details  
300 are given in Appendix A.

301  
302 **Models, Datasets, and Compute.** We evaluate on a diverse set of medical benchmarks that span  
303 vision (Brain MRI (Nickparvar, 2021), Chest X-ray (CheXpert) (Irvin et al., 2019), and Breast  
304 Cancer Histopathology (BreakHis) (Spanhol et al., 2015)), language (MedQA (Jin et al., 2021), MedM-  
305 CQA (Pal et al., 2022)), and tabular domains (PhysioNet (Haug et al., 2021), Breast Cancer (Wolberg  
306 et al., 1993), Cardiotocography (CTG) (Campos & Bernardes, 2000)). We respectively evaluate on  
307 these domains with ViT-B/16 (Dosovitskiy et al., 2020), Llama-3.1-8B-Instruct (AI@Meta, 2024),  
308 and XGBoost (Chen & Guestrin, 2016), which are trained using standard methods. For compute,  
309 we had access to a machine with four NVIDIA H100 NVL GPUs.  
310

311  
312 **Input Ablations and Calibration.** We say that an input  $x \in \mathbb{R}^n$  has ablation rate  $p = k/n$  if  $k$  of  
313 its features are ablated. To evaluate on a tractable range of  $p$ , we use  $p \in \{0/16, 1/16, \dots, 15/16\}$   
314 for vision,  $p \in \{0/10, 1/10, \dots, 9/10\}$  for language, and  $p \in \{0/10, 1/10, \dots, 9/10\}$  for tabular,  
315 where recall that we recover the clean input at  $p = 0$ . For imputations, we use zero-valued (black)  
316 patches for vision, we replace whitespace-separated words with the special string UNKWORDS for  
317 language, and we perform mean imputation for tabular data. For vision specifically, we select  $k$   
318 patches to ablate, regardless of their original values (e.g., some MRI images already have black  
319 patches). Following discussion from Section 3.3, the *unconditioned* calibrator was fit on inputs  
320 where each feature was uniformly ablated with probability 1/2, whereas the *conditioned* ensemble  
321 has a calibrator fit at each value of  $p$ . All calibrators were optimized using Adam (Kingma & Ba,  
322 2014) with a learning rate of  $10^{-3}$  for 5000 steps.

323  
324 **Question 1: Do calibrated models lead to better explanations?** Missingness bias is known to  
325 skew the explanation quality of feature attribution methods (Jain et al., 2022). To that end, we con-  
326 sider how two representative methods, LIME (Ribeiro et al., 2016) and SHAP (Lundberg & Lee,

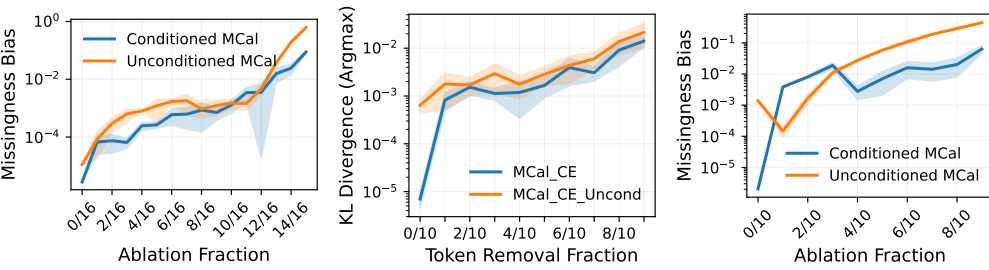


Figure 6: **Conditioning on ablation rate improves MCal.** Fitting an ensemble of calibrators at a discretized set of ablation rates can help reduce the overall missingness rate, compared to using a single unconditioned calibrator. (Left) MRI, (Middle) MedQA, (Right) PhysioNet.

	<b>Dataset</b>	<b>Original</b>	<b>Replace</b>	<b>Retrain</b>	<b>Arch</b>	<b>TempCal</b>	<b>PlattCal</b>	<b>MCal (✓)</b>
<b>Vision</b>	Brain MRI	1.18 e-1	1.51 e-1	<b>6.70 e-4</b>	1.40 e-1	1.16 e-1	1.27 e-1	7.43 e-3
	CheXpert	1.70 e-1	9.70 e-2	2.67 e-2	1.50 e-1	1.65 e-1	2.02 e-1	<b>8.82 e-3</b>
	BreakHis	1.87 e-1	4.20 e-1	2.19 e-2	1.54 e-1	1.86 e-1	1.66 e-1	<b>4.29 e-3</b>
<b>Language</b>	MedQA	1.61 e-1	1.50 e-1	1.70 e-1	2.68 e-2	1.57 e-1	9.48 e-2	<b>9.44 e-4</b>
	MedMCQA	1.89 e-1	2.59 e-1	1.52 e-1	1.40 e-1	7.81 e-1	1.13 e-1	<b>9.01 e-3</b>
<b>Tabular</b>	PhysioNet	1.17 e-1	1.20 e-1	5.59 e-3	8.14 e-2	1.17 e-1	1.19 e-1	<b>5.01 e-3</b>
	Breast Cancer	1.02 e-1	1.44 e-1	5.68 e-3	2.13 e-1	1.02 e-1	1.08 e-1	<b>1.92 e-5</b>
	CTG	1.06 e-1	7.02 e-2	6.61 e-3	2.85 e-1	1.06 e-1	9.20 e-2	<b>3.35 e-3</b>

Table 1: **MCal is an effective and lightweight way to reduce missingness bias.** It repeatedly outperforms more computationally expensive baselines, such as retraining and architecture modification. We report the KL divergence-based metric in Equation (1).

2017), perform on calibrated vs. uncalibrated models. These methods output a ranking of each input feature’s importance to the model, which we evaluate using the standard *sufficiency* metric (Hase et al., 2021), detailed in Appendix A.1. Informally, sufficiency measures whether the features identified as important are enough on their own to maintain the model’s original prediction confidence (lower values indicate a higher quality ranking). We report results in Figure 5.

**Question 2: How does calibration affect model robustness?** It is generally desirable for models to be robust to feature perturbations, as this can improve generalization and reduce the risk of adversarial behaviors. To that end, we measure the robustness of the underlying model to the removal (ablation) of features via the *sensitivity* metric, detailed in Figure 5. We show our results in Appendix A.1, which shows that the model is not overly dependent on its top-k features for prediction.

**Question 3: What is the impact of conditioning on feature ablation fractions?** Rather than fitting a single calibrator, we observe that using an ensemble of calibrators, each conditioned upon a single fraction (ablation rate), can improve performance. We compare the performance of this conditioning in Figure 6, where we observe an improvement in performance over an unconditioned calibrator. This is expected, as a model’s missingness bias is known to vary with the ablation rate (Hooker et al., 2019; Jain et al., 2022), and an ensemble thereby allows each calibrator to specialize to their respective rates.

**Question 4: How does MCal compare to the baselines?** We compare MCal to each of the following prior approaches which have all been employed in previous work to combat the problem of out of distribution inputs

- **Original:** This is the unmodified, uncalibrated classifier that acts as a reference baseline.
- **Replacement-based (Replace):** Our implementation of replacement-based mitigation is inspired from Hase et al. (2021). In particular, for vision, we use the channel-wise mean pixel value of the clean dataset (Carter et al., 2021). For language, we drop tokens from the sequence

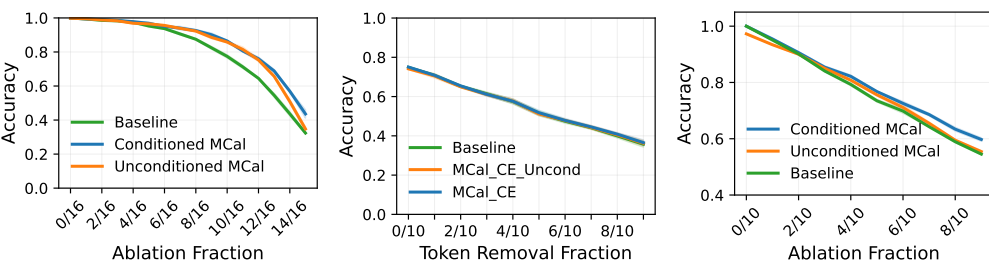


Figure 7: **MCAL does not harm classifier accuracy.** Across different ablation levels, the accuracy of uncalibrated vs. calibrated classifiers is comparable. This also holds when the input is clean (ablation fraction zero). (Left) MRI, (Middle) MedQA, (Right) PhysioNet.

so that the ablated token sequence is shorter in length than the clean one (Hase et al., 2021). For tabular, we perform mean imputation.

- **Training-based approaches (Retrain):** Models are fine-tuned on ablated inputs, where each feature (patch, token) is uniformly ablated with probability 1/2.
- **Architectural-based (Arch):** We perform a non-trivial modification of ViT to accept attention masks as in Jain et al. (2022). For models with architectural support for missing features, we use those: e.g., attention masking in Llama-3 and native support for NaN in XGBoost.
- **Standard calibration (TempCal, PlattCal):** We additionally consider existing calibration-based methods from literature, particularly temperature (TempCal) and vector-scaling Platt calibration (PlattCal), as described in Guo et al. (2017).

We report in Table 1 the average of values from the ensemble of conditioned calibrators. We found that MCAL is often superior even to more computationally and engineering-intensive baselines, such as model retraining and ViT architecture modifications. In support of our earlier claims, we also observe that MCAL outperforms both temperature and Platt calibration. Replacement-based methods have inconsistent performance, which aligns with known observations on their sensitivity to imputation values. Finally, we note that architecture-native support for missing features may, in fact, exacerbate missingness bias, as seen in XGBoost on the Breast Cancer and CTG datasets.

**Question 5: How does MCAL affect classifier accuracy?** MCAL fundamentally alters a pretrained base classifier  $f$  into  $\tilde{f}$ , which is then deployed to downstream applications. Importantly, the accuracy of  $\tilde{f}$  must remain high, even when it is optimized on ablated images Equation (3). We show in Figure 7 that this is indeed the case: we compare the uncalibrated base model against both ablation rate-conditioned and unconditioned calibrators. We observe that both forms of calibration improve classifier accuracy at all ablation rates, where we recall that the clean image is obtained at an ablation rate of zero. Aligning with earlier findings, we see that the conditioned calibrator outperforms the unconditioned calibrator.

## 5 RELATED WORK

**Missingness Bias in Explainability.** Missingness bias (Jain et al., 2022) denotes the systematic distortions that arise when attribution methods “remove” features via ablations, e.g., with black pixels, zero-valued embeddings, or special [MASK] tokens. Such ablated inputs are often out-of-distribution with respect to the model’s training distribution, which can result in erratic predictions, inflated confidences, and unstable feature importance scores (Hooker et al., 2019; Vo et al., 2024). In particular, importance scores can vary drastically with the chosen replacement technique (Haug et al., 2021; Sturmels et al., 2020) and can even be exploited adversarially (Slack et al., 2020). Consequently, feature-based explanations commonly reflect ablation artifacts rather than genuine model reasoning (Hase et al., 2021), which risks eroding trust in high-stakes settings. In addition to the methods described earlier in Section 2.2, there are several benchmarks related to missingness bias (Duan et al., 2024; Hesse et al., 2023; Liu et al., 2021).

---

432     **Calibration Methods.** A calibration method post-hoc rescales the logits or probabilities of a  
433     model prediction without modifying the underlying model weights. Classic techniques include bin-  
434     ning (Zadrozny & Elkan, 2001), Platt scaling (Platt et al., 1999), and temperature scaling (Guo et al.,  
435     2017). This is often used to improve and calibrate model predictions under input distribution shift,  
436     such as in autonomous driving (Tomani et al., 2021), healthcare (Shashikumar et al., 2023), and  
437     LLMs (Kumar et al., 2022). To our knowledge, however, calibration for missingness bias is novel.  
438

439     **Robust and Reliable Explanations.** There is much interest in the development of robust expla-  
440     nations for machine learning models. Notable efforts include the development of benchmarks for  
441     explanations, particularly feature attribution methods (Adebayo et al., 2018; 2022; Agarwal et al.,  
442     2022; Dinu et al., 2020; Duan et al., 2024; Jin et al., 2024; Kindermans et al., 2019; Nauta et al.,  
443     2023; Rong et al., 2022; Zhou et al., 2022). There is also interest in formally certifying expla-  
444     nations (Bassan & Katz, 2023; Bassan et al., 2025; Jin et al., 2025; Lin et al., 2023; Xue et al., 2023;  
445     You et al., 2025). Other efforts, such as this work, involve adapting classifiers to be more robust to  
446     input ablations in feature attributions.  
447

## 448     6 DISCUSSION, FUTURE DIRECTIONS, AND CONCLUSION

449  
450     **Calibration Design.** While other calibrator parametrizations are viable, any non-convex  
451     parametrization of the objective risks losing guarantees of optimality convergence. In turn, this  
452     risks introducing undesirable behavior, such as sensitivity to the initialization of calibrator parame-  
453     ters. Additionally, observe that the measure of missingness bias (Equation (1)) is different than the  
454     calibrator optimization objective. This is because the missingness bias measure is not differentiable  
455     due to the one-hot Class function, which motivated us to search for reasonable alternatives, e.g.,  
456     the standard cross-entropy objective in classification. While it would be interesting to explore, for  
457     instance, differentiable relaxations of Equation (1), we leave this to future work.  
458

459     **Missingness Bias and Data Variability.** Visual medical datasets, e.g., Chest X-rays, often exhibit  
460     lower variability than image datasets like ImageNet (Deng et al., 2009). Despite this, missingness  
461     bias can persist in models trained on datasets such as ImageNet (Jain et al., 2022). However, it is not  
462     known how missingness bias varies as a function of both dataset variability and model architecture.  
463

464     **Beyond Explainability.** Missingness bias is a fundamental risk when evaluating feature subsets  
465     on a model that is not explicitly designed to handle missing data. While we are primarily motivated  
466     by challenges in explainability, this work has broader applications. In vision, model evaluation  
467     with masked images is a standard practice. In language modeling, a token’s embedding is often  
468     dependent on its position, meaning that ablations are position-sensitive, whether via the attention  
469     mask, subsetting the input sequence, or replacement with special [MASK] tokens.  
470

471     **Limitations.** MCal requires access to a collection of clean and ablated prediction logits, which  
472     may not always be available, such as for some API-based LLMs. Even then, gradient-based opti-  
473     mization is only guaranteed to converge to global optimality under certain parameterizations of the  
474     calibrator. Overfitting is also a potential risk, particularly in settings with a large number of possible  
475     classes (e.g., a language model’s vocabulary size), in which case regularization is warranted. Fur-  
476     thermore, MCal is only intended to mitigate missingness bias, and other forms of bias in the model  
477     and data may still be propagated. While our experiments show that linear corrections on the logits  
478     suffice to mitigate missingness bias, and hence our use of the description “superficial”, it may be the  
479     case that for missingness bias in certain model classes, it is harder to mitigate in this manner.  
480

481     **Future Work.** One direction is to investigate the theoretical guarantees and empirical performance  
482     of different calibrator parametrizations, such as a one-layer feedforward network instead of an affine  
483     transform. Another extension is to broaden our study on the performance of calibrated classifiers in  
484     explainability, such as with respect to the explanation methods and metrics surveyed in Section 5. It  
485     would be interesting to explore methods for mitigating missingness bias when prediction logits are  
486     not available, a common restriction for API-based large language models. Additionally, the idea of  
487     calibration may also be extended to other instances of domain shift and Out of Distribution inputs,  
488     which are prevalent throughout Machine Learning literature  
489

---

486     **Conclusion.** Missingness bias threatens the reliability of popular explanation methods and techniques, a problem magnified by the increasing impracticality of existing engineering-intensive solutions.  
487     To overcome this, we introduce MCAL, a lightweight calibration method that requires only a  
488     collection of clean and ablated prediction pairs. We demonstrate that a simple, affine parametrization  
489     of the calibrator offers strong theoretical guarantees while achieving empirical performance  
490     that often outperforms more expensive baselines. In summary, MCAL is an efficient, model-agnostic  
491     calibration scheme that improves the reliability of popular feature-based explanation methods.  
492

493     **Ethics Statement.** This work presents a method for improving the reliability of feature-based  
494     explanation methods. Our intended audience includes researchers and practitioners interested in  
495     explainability. While there may be potential for misuse, we do not believe that the contents of this  
496     paper warrant concern.  
497

498     **Reproducibility Statement.** All code and experiments for this paper are available at:  
499

500         <https://anonymous.4open.science/r/MCal-DE3C/>  
501  
502

## 503 REFERENCES

- 504     Julius Adebayo, Justin Gilmer, Michael Muelly, Ian Goodfellow, Moritz Hardt, and Been Kim.  
505     Sanity checks for saliency maps. *Advances in neural information processing systems*, 31, 2018.
- 506     Julius Adebayo, Michael Muelly, Harold Abelson, and Been Kim. Post hoc explanations may be  
507     ineffective for detecting unknown spurious correlation. In *International conference on learning*  
508     *representations*, 2022.
- 509     Chirag Agarwal and Anh Nguyen. Explaining image classifiers by removing input features using  
510     generative models. *arXiv preprint arXiv:1910.04256*, 2020.
- 511     Chirag Agarwal, Satyapriya Krishna, Eshika Saxena, Martin Pawelczyk, Nari Johnson, Isha Puri,  
512     Marinka Zitnik, and Himabindu Lakkaraju. Openxai: Towards a transparent evaluation of model  
513     explanations. *Advances in neural information processing systems*, 35:15784–15799, 2022.
- 514     AI@Meta. Llama 3 model card, 2024. URL [https://github.com/meta-llama/llama3/  
515     blob/main/MODEL\\_CARD.md](https://github.com/meta-llama/llama3/blob/main/MODEL_CARD.md).
- 516     Marco Ancona, Enea Ceolini, Cengiz Öztireli, and Markus Gross. Towards better understanding of  
517     gradient-based attribution methods for deep neural networks. *arXiv preprint arXiv:1711.06104*,  
518     2017.
- 519     Sriram Balasubramanian and Soheil Feizi. Towards improved input masking for convolutional neu-  
520     ral networks. In *Proceedings of the IEEE/CVF International Conference on Computer Vision*, pp.  
521     1855–1865, 2023.
- 522     Shahaf Bassan and Guy Katz. Towards formal xai: formally approximate minimal explanations of  
523     neural networks. In *International Conference on Tools and Algorithms for the Construction and*  
524     *Analysis of Systems*, pp. 187–207. Springer, 2023.
- 525     Shahaf Bassan, Guy Amir, Meirav Zehavi, and Guy Katz. What makes an ensemble (un) inter-  
526     pretable? *arXiv e-prints*, pp. arXiv–2506, 2025.
- 527     D. Campos and J. Bernardes. Cardiotocography. UCI Machine Learning Repository, 2000. DOI:  
528     <https://doi.org/10.24432/C51S4N>.
- 529     Brandon Carter, Siddhartha Jain, Jonas W Mueller, and David Gifford. Overinterpretation reveals  
530     image classification model pathologies. *Advances in Neural Information Processing Systems*, 34:  
531     15395–15407, 2021.
- 532     Chun-Hao Chang, Elliot Creager, Anna Goldenberg, and David Duvenaud. Explaining image clas-  
533     sifiers by counterfactual generation. *arXiv preprint arXiv:1807.08024*, 2018.

- 
- 540 Tianqi Chen and Carlos Guestrin. Xgboost: A scalable tree boosting system. In *Proceedings of the*  
541 *22nd ACM SIGKDD international conference on knowledge discovery and data mining*, pp. 785–794,  
542 2016.
- 543 Nadezhda Chirkova, Germán Kruszewski, Jos Rozen, and Marc Dymetman. Should you marginalize  
544 over possible tokenizations? *arXiv preprint arXiv:2306.17757*, 2023.
- 545 Jia Deng, Wei Dong, Richard Socher, Li-Jia Li, Kai Li, and Li Fei-Fei. Imagenet: A large-scale hi-  
546 erarchical image database. In *2009 IEEE conference on computer vision and pattern recognition*,  
547 pp. 248–255. Ieee, 2009.
- 548 Jonathan Dinu, Jeffrey Bigham, and J Zico Kolter. Challenging common interpretability assump-  
549 tions in feature attribution explanations. *arXiv preprint arXiv:2012.02748*, 2020.
- 550 Alexey Dosovitskiy, Lucas Beyer, Alexander Kolesnikov, Dirk Weissenborn, Xiaohua Zhai, Thomas  
551 Unterthiner, Mostafa Dehghani, Matthias Minderer, Georg Heigold, Sylvain Gelly, et al. An  
552 image is worth 16x16 words: Transformers for image recognition at scale. *arXiv preprint*  
553 *arXiv:2010.11929*, 2020.
- 554 Jiarui Duan, Haoling Li, Haofei Zhang, Hao Jiang, Mengqi Xue, Li Sun, Mingli Song, and Jie  
555 Song. On the evaluation consistency of attribution-based explanations. In *European Conference*  
556 *on Computer Vision*, pp. 206–224. Springer, 2024.
- 557 Christopher Frye, Damien de Mijolla, Tom Begley, Laurence Cowton, Megan Stanley, and Ilya  
558 Feige. Shapley explainability on the data manifold. *arXiv preprint arXiv:2006.01272*, 2020.
- 559 Jeremy Goldwasser and Giles Hooker. Provably stable feature rankings with shap and lime. *arXiv*  
560 *preprint arXiv:2401.15800*, 2024.
- 561 Chuan Guo, Geoff Pleiss, Yu Sun, and Kilian Q Weinberger. On calibration of modern neural  
562 networks. In *International conference on machine learning*, pp. 1321–1330. PMLR, 2017.
- 563 Peter Hase, Harry Xie, and Mohit Bansal. The out-of-distribution problem in explainability and  
564 search methods for feature importance explanations. *Advances in neural information processing*  
565 *systems*, 34:3650–3666, 2021.
- 566 Johannes Haug, Stefan Zürn, Peter El-Jiz, and Gjergji Kasneci. On baselines for local feature attri-  
567 butions. *arXiv preprint arXiv:2101.00905*, 2021.
- 568 Robin Hesse, Simone Schaub-Meyer, and Stefan Roth. Funnybirds: A synthetic vision dataset for  
569 a part-based analysis of explainable ai methods. In *Proceedings of the IEEE/CVF International*  
570 *Conference on Computer Vision*, pp. 3981–3991, 2023.
- 571 Sara Hooker, Dumitru Erhan, Pieter-Jan Kindermans, and Been Kim. A benchmark for interpretabil-  
572 ity methods in deep neural networks. *Advances in neural information processing systems*, 32,  
573 2019.
- 574 Edward J Hu, Yelong Shen, Phillip Wallis, Zeyuan Allen-Zhu, Yuanzhi Li, Shean Wang, Lu Wang,  
575 Weizhu Chen, et al. Lora: Low-rank adaptation of large language models. *ICLR*, 1(2):3, 2022.
- 576 Jeremy Irvin, Pranav Rajpurkar, Michael Ko, Yifan Yu, Silviana Ciurea-Illcus, Chris Chute, Henrik  
577 Marklund, Behzad Haghgoo, Robyn Ball, Katie Shpanskaya, et al. Chexpert: A large chest  
578 radiograph dataset with uncertainty labels and expert comparison. In *Proceedings of the AAAI*  
579 *conference on artificial intelligence*, volume 33, pp. 590–597, 2019.
- 580 Saachi Jain, Hadi Salman, Eric Wong, Pengchuan Zhang, Vibhav Vineet, Sai Venkrala, and Alek-  
581 sander Madry. Missingness bias in model debugging. *arXiv preprint arXiv:2204.08945*, 2022.
- 582 Di Jin, Eileen Pan, Nassim Oufattolle, Wei-Hung Weng, Hanyi Fang, and Peter Szolovits. What dis-  
583 ease does this patient have? a large-scale open domain question answering dataset from medical  
584 exams. *Applied Sciences*, 11(14):6421, 2021.
- 585 Helen Jin, Shreya Havaldar, Chaehyeon Kim, Anton Xue, Weiqiu You, Helen Qu, Marco Gatti,  
586 Daniel A Hashimoto, Bhuvnesh Jain, Amin Madani, et al. The fix benchmark: Extracting features  
587 interpretable to experts. *arXiv preprint arXiv:2409.13684*, 2024.

- 
- 594 Helen Jin, Anton Xue, Weiqiu You, Surbhi Goel, and Eric Wong. Probabilistic stability guarantees  
595 for feature attributions. *arXiv preprint arXiv:2504.13787*, 2025.
- 596
- 597 Byunggill Joe, Yonghyeon Park, Jihun Hamm, Insik Shin, Jiyeon Lee, et al. Exploiting missing  
598 value patterns for a backdoor attack on machine learning models of electronic health records:  
599 Development and validation study. *JMIR Medical Informatics*, 10(8):e38440, 2022.
- 600
- 601 Siwon Kim, Jihun Yi, Eunji Kim, and Sungroh Yoon. Interpretation of nlp models through input  
602 marginalization. In *Proceedings of the 2020 Conference on Empirical Methods in Natural Lan-*  
603 *guage Processing (EMNLP)*, pp. 3154–3167, 2020.
- 604
- 605 Pieter-Jan Kindermans, Sara Hooker, Julius Adebayo, Maximilian Alber, Kristof T Schütt, Sven  
606 Dähne, Dumitru Erhan, and Been Kim. The (un)reliability of saliency methods. *Explainable AI: Interpreting, explaining and visualizing deep learning*, pp. 267–280, 2019.
- 607
- 608 Diederik P Kingma and Jimmy Ba. Adam: A method for stochastic optimization. *arXiv preprint arXiv:1412.6980*, 2014.
- 609
- 610 Deniz Koyuncu, Alex Gittens, Bülent Yener, and Moti Yung. Exploiting the data gap: Utilizing non-  
611 ignorable missingness to manipulate model learning. *arXiv preprint arXiv:2409.04407*, 2024.
- 612
- 613 Ananya Kumar, Tengyu Ma, Percy Liang, and Aditi Raghunathan. Calibrated ensembles can mit-  
614 igate accuracy tradeoffs under distribution shift. In *Uncertainty in Artificial Intelligence*, pp.  
615 1041–1051. PMLR, 2022.
- 616
- 617 Chris Lin, Ian Covert, and Su-In Lee. On the robustness of removal-based feature attributions.  
618 *Advances in Neural Information Processing Systems*, 36:79613–79666, 2023.
- 619
- 620 Yang Liu, Sujay Khandagale, Colin White, and Willie Neiswanger. Synthetic benchmarks for sci-  
621 entific research in explainable machine learning. *arXiv preprint arXiv:2106.12543*, 2021.
- 622
- 623 Scott M Lundberg and Su-In Lee. A unified approach to interpreting model predictions. *Advances in neural information processing systems*, 30, 2017.
- 624
- 625 Meike Nauta, Jan Trienes, Shreyasi Pathak, Elisa Nguyen, Michelle Peters, Yasmin Schmitt, Jörg  
626 Schlötterer, Maurice Van Keulen, and Christin Seifert. From anecdotal evidence to quantitative  
627 evaluation methods: A systematic review on evaluating explainable ai. *ACM Computing Surveys*,  
628 55(13s):1–42, 2023.
- 629
- 630 Msoud Nickparvar. Brain tumor mri dataset, 2021. URL <https://www.kaggle.com/dsv/2645886>.
- 631
- 632 Ankit Pal, Logesh Kumar Umapathi, and Malaikannan Sankarasubbu. Medmcqa: A large-scale  
633 multi-subject multi-choice dataset for medical domain question answering. In *Conference on health,*  
634 *inference, and learning*, pp. 248–260. PMLR, 2022.
- 635
- 636 Yong-Hyun Park, Junghoon Seo, Bomseok Park, Seongsu Lee, and Junghyo Jo. Geometric  
637 remove-and-retrain (goar): Coordinate-invariant explainable ai assessment. *arXiv preprint arXiv:2407.12401*, 2024.
- 638
- 639 John Platt et al. Probabilistic outputs for support vector machines and comparisons to regularized  
640 likelihood methods. *Advances in large margin classifiers*, 10(3):61–74, 1999.
- 641
- 642 Marco Tulio Ribeiro, Sameer Singh, and Carlos Guestrin. ” why should i trust you?” explaining the  
643 predictions of any classifier. In *Proceedings of the 22nd ACM SIGKDD international conference on knowledge discovery and data mining*, pp. 1135–1144, 2016.
- 644
- 645 Yao Rong, Tobias Leemann, Vadim Borisov, Gjergji Kasneci, and Enkelejda Kasneci. A consistent  
646 and efficient evaluation strategy for attribution methods. *arXiv preprint arXiv:2202.00449*, 2022.
- 647
- 648 Supreeth P Shashikumar, Fatemeh Amrollahi, and Shamim Nemat. Unsupervised detection and  
649 correction of model calibration shift at test-time. In *2023 45th Annual International Conference of the IEEE Engineering in Medicine & Biology Society (EMBC)*, pp. 1–4. IEEE, 2023.

- 
- 648 Dylan Slack, Sophie Hilgard, Emily Jia, Sameer Singh, and Himabindu Lakkaraju. Fooling lime  
649 and shap: Adversarial attacks on post hoc explanation methods. In *Proceedings of the AAAI/ACM*  
650 *Conference on AI, Ethics, and Society*, pp. 180–186, 2020.
- 651
- 652 Fabio A Spanhol, Luiz S Oliveira, Caroline Petitjean, and Laurent Heutte. A dataset for breast  
653 cancer histopathological image classification. *Ieee transactions on biomedical engineering*, 63  
654 (7):1455–1462, 2015.
- 655 Pascal Sturmels, Scott Lundberg, and Su-In Lee. Visualizing the impact of feature attribution  
656 baselines. *Distill*, 5(1):e22, 2020.
- 657
- 658 Mukund Sundararajan, Ankur Taly, and Qiqi Yan. Axiomatic attribution for deep networks. In  
659 *International conference on machine learning*, pp. 3319–3328. PMLR, 2017.
- 660 Christian Tomani, Sebastian Gruber, Muhammed Ebrar Erdem, Daniel Cremers, and Florian Buet-  
661 tner. Post-hoc uncertainty calibration for domain drift scenarios. In *Proceedings of the IEEE/CVF*  
662 *Conference on Computer Vision and Pattern Recognition*, pp. 10124–10132, 2021.
- 663
- 664 Tuan L Vo, Thu Nguyen, Luis M Lopez-Ramos, Hugo L Hammer, Michael A Riegler, and Pal  
665 Halvorsen. Explainability of machine learning models under missing data. *arXiv preprint*  
666 *arXiv:2407.00411*, 2024.
- 667
- 668 William Wolberg, Olvi Mangasarian, Nick Street, and W. Street. Breast Cancer Wisconsin (Diag-  
nostic). UCI Machine Learning Repository, 1993. DOI: <https://doi.org/10.24432/C5DW2B>.
- 669
- 670 Anton Xue, Rajeev Alur, and Eric Wong. Stability guarantees for feature attributions with mul-  
671 tiplicative smoothing. *Advances in Neural Information Processing Systems*, 36:62388–62413,  
672 2023.
- 673
- 674 Weiqiu You, Anton Xue, Shreya Havaldar, Delip Rao, Helen Jin, Chris Callison-Burch, and  
675 Eric Wong. Probabilistic soundness guarantees in llm reasoning chains. *arXiv preprint*  
676 *arXiv:2507.12948*, 2025.
- 677
- 678 Bianca Zadrozny and Charles Elkan. Obtaining calibrated probability estimates from decision trees  
679 and naive bayesian classifiers. In *Proceedings of the Eighteenth International Conference on*  
680 *Machine Learning*, pp. 609–616, 2001.
- 681
- 682 Yilun Zhou, Serena Booth, Marco Tulio Ribeiro, and Julie Shah. Do feature attribution methods  
683 correctly attribute features? In *Proceedings of the AAAI conference on artificial intelligence*,  
684 volume 36, pp. 9623–9633, 2022.
- 685
- 686
- 687
- 688
- 689
- 690
- 691
- 692
- 693
- 694
- 695
- 696
- 697
- 698
- 699
- 700
- 701

---

702     A ADDITIONAL EXPERIMENTS AND DETAILS  
703

704     We present our experimental setup here, along with any additional experiments and relevant details.  
705

706     **Compute.** We had access to a server with four NVIDIA H100 NVL GPUs.  
707

708     A.1 OTHER METRICS RELATED TO MISSINGNESS BIAS  
709

710     Given an input  $x \in \mathbb{R}^n$  and a classifier  $f : \mathbb{R}^n \rightarrow \mathbb{R}$ , an explanation method returns a ranking  $\alpha \in \mathbb{R}^n$  of each feature's importance. To evaluate the quality of  $\alpha$ , we use the *sufficiency* and *sensitivity* metrics (Hase et al., 2021), which measure how model confidence changes when important features are isolated or removed.

714     From the scores  $\alpha$ , we create a binary mask  $e_k \in \{0, 1\}^n$  selecting the top- $k$  most important features.  
715     The sufficiency metric evaluates if this subset of features is sufficient to yield the original prediction.  
716

$$717 \quad \text{Sufficiency}(f, x, e_k) = f(x_{\hat{y}}) - f(\text{Replace}(x, e_k))_{\hat{y}} \quad (4)$$

718     Here,  $\hat{y} = \arg \max_y f(x)_y$  is the predicted class. The  $\text{Replace}(x, e_k)$  function creates a counterfac-  
719     tual by preserving only the top- $k$  features against a baseline. A lower score is better, indicating the  
720     selected features are sufficient.

721     Conversely, the sensitivity metric (called *comprehensiveness* in Hase et al. (2021)) evaluates if im-  
722     portant features are necessary for the prediction by measuring the confidence drop upon their re-  
723     moval.

$$724 \quad \text{Sensitivity}(f, x, e_k) = f(x_{\hat{y}}) - f(\text{Replace}(x, \neg e_k))_{\hat{y}} \quad (5)$$

725     The top- $k$  features in mask  $e_k$  are removed by preserving those in the complement mask  $\neg e_k$ . A  
726     higher score indicates the features were critical to the prediction. A lower score suggests the model  
727     is more robust to their exclusion.  
728

729     A.2 MCAL TRAINING DYNAMICS  
730

731     Here, we investigate the training dynamics and performance of MCAL as the training set size varies.  
732     We show the results in Figure 8. In general, as the training dataset size increases, test-time accuracy  
733     increases. When  $n$  is small, however, the problem is over-parametrized, meaning that the training  
734     loss continues to decrease without significantly improving test-time accuracy.

735     A.3 CASE STUDY: INTEGRATION WITH API-BASED MODELS  
736

738     Current day Machine Learning research is becoming increasingly dependent on popular closed-  
739     weight API-based models, such as those offered by OpenAI, Anthropic, OpenRouter etc. Recogniz-  
740     ing this, we perform a case study demonstrating how MCAL can be extended to such models, only  
741     requiring log-probabilities to work.

742     Using the GPT-4o-mini API and selected MedQA questions, we demonstrate MCAL integration in  
743     our repository notebook. The calibrated model redistributes feature importance in potentially mean-  
744     ingful ways - elevating diagnostic symptoms like “hematuria”(a hallmark sign of cyclophosphamide  
745     toxicity) and “pain”, while reducing dominance of the anatomical term “suprapubic”. This rebal-  
746     ancing suggests calibration may produce more clinically-aligned and faithful explanations, though  
747     domain expert validation and further faithfulness testing is needed to confirm this. See Figure 9 and  
748     Figure 10.

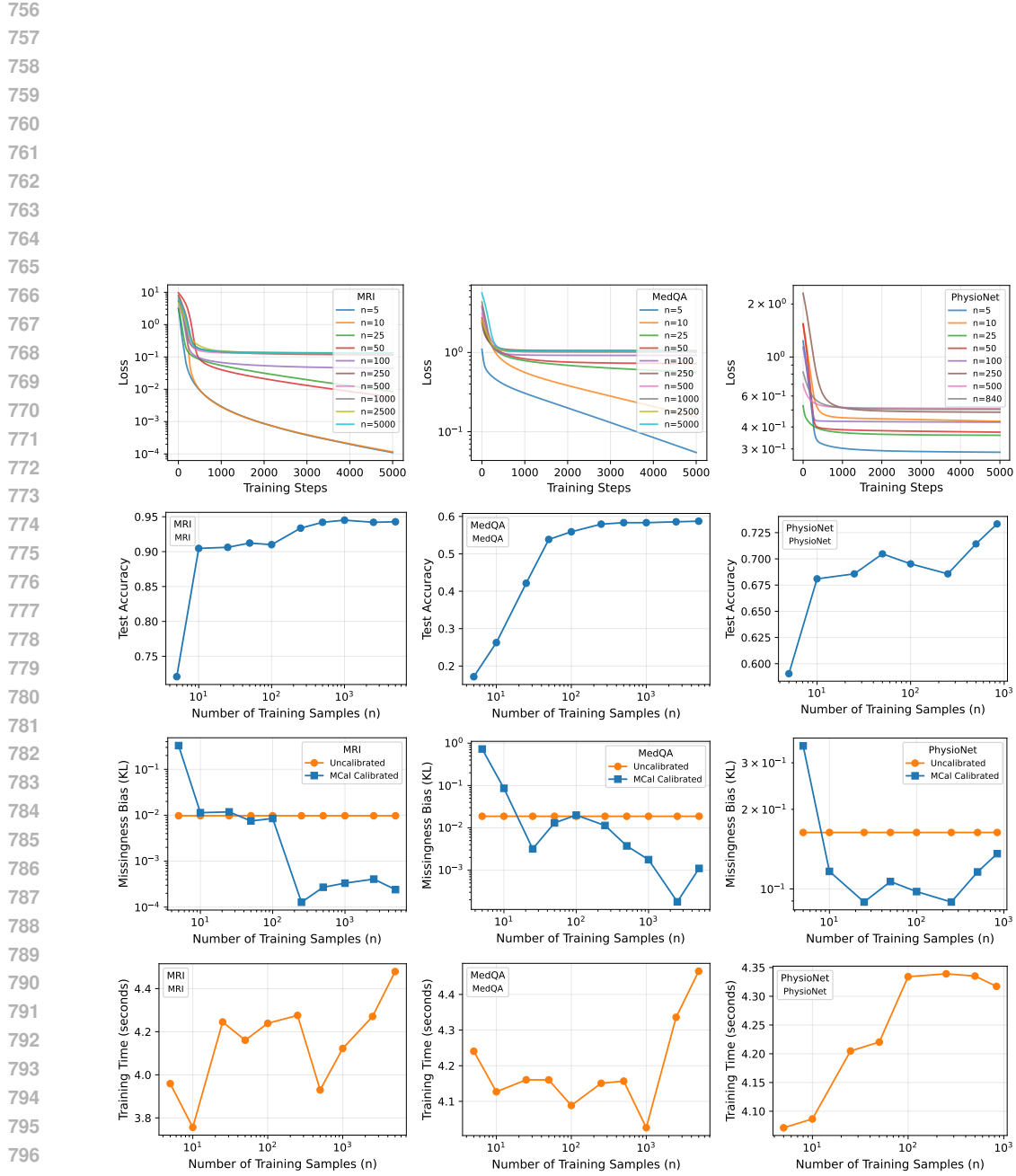
749     B ADDITIONAL FIGURES  
750

751     We include additional figures in this section.  
752

753

754

755



810  
811  
812  
813  
814  
815  
816  
817  
818

819  
820  
821  
822  
823

824  
825  
826  
827  
828  
829  
830  
831  
832  
833  
834  
835  
836  
837  
838  
839  
840

841  
842  
843  
844

845  
846  
847

849

851

852

854

855

856

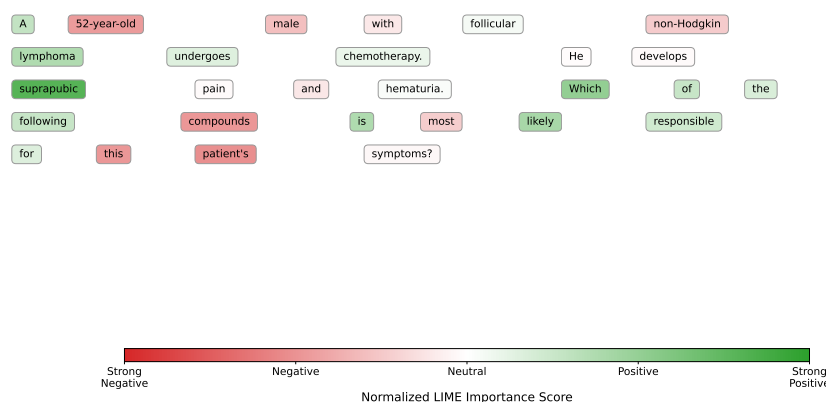
858

859

861

862

### **Baseline (Uncalibrated) LIME Explanation for "A"**



### Unconditioned MCal (Calibrated) LIME Explanation for "A"

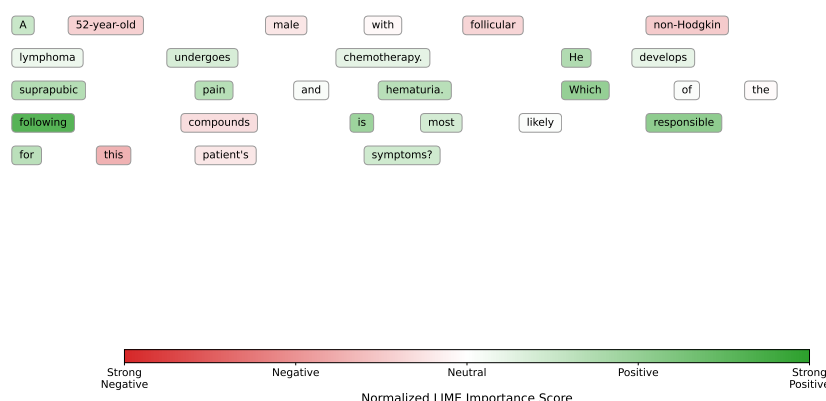


**Figure 9: For a selected example question, MCal results in different feature importances**, for example medically relevant features/terms such as "hematuria" gain importance in the calibrated heatmap. The model task is, for the above question, to choose between the Options: A: Cyclophosphamide, B: Cisplatin, C: Mesna, D: Bleomycin.

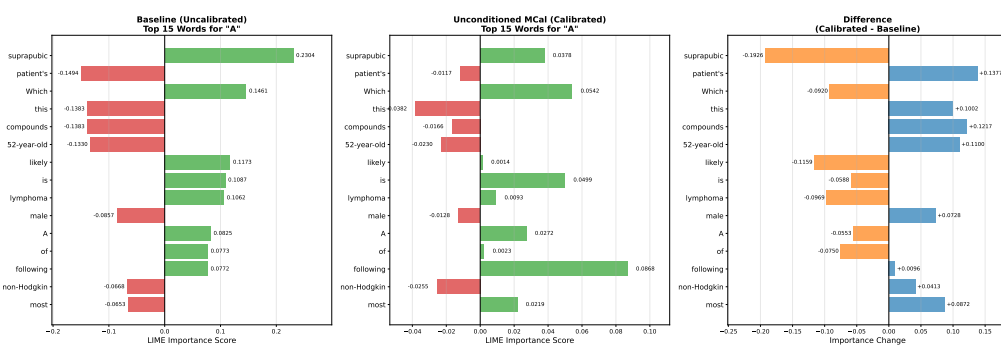


Figure 10: Direct comparison of LIME-derived feature importance values, with (a) Uncalibrated, (b) Calibrated, and (c) demonstrating the difference between the two, i.e., (b) - (a).

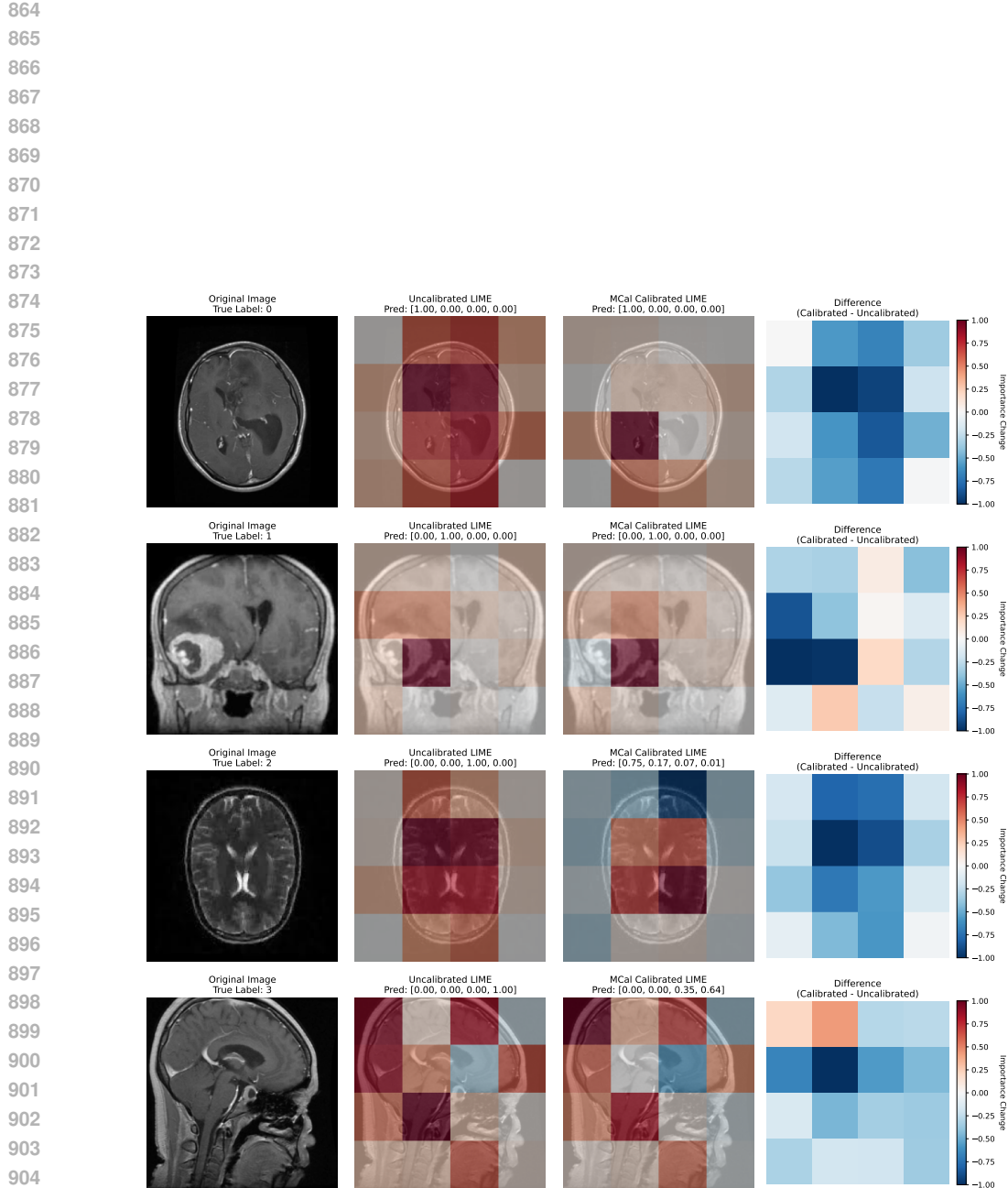


Figure 11: **Selected examples of LIME on the MRI dataset.** In calibrated models, we observe that LIME tends to assign less importance to border patches, where relevant features are less likely to occur. The four classes are: Meningioma (0), Glioma (1), Pituitary Tumor (2), and No Tumor (3).

```

906
907
908
909
910
911
912
913
914
915
916
917
```